

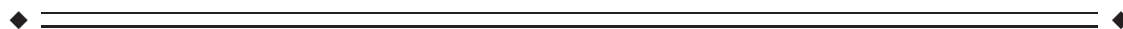
Addressing a Systematic Vibration Artifact in Diffusion-Weighted MRI

Daniel Gallichan,^{1*} Jan Scholz,¹ Andreas Bartsch,² Timothy E. Behrens,¹ Matthew D. Robson,³ and Karla L. Miller¹

¹Centre for Functional Magnetic Resonance Imaging of the Brain, John Radcliffe Hospital, University of Oxford, Oxford, United Kingdom

²Department of Neuroradiology, University of Würzburg, Würzburg, Germany

³University of Oxford Centre for Clinical Magnetic Resonance Research, Oxford, United Kingdom



Abstract: We have identified and studied a pronounced artifact in diffusion-weighted MRI on a clinical system. The artifact results from vibrations of the patient table due to low-frequency mechanical resonances of the system which are stimulated by the low-frequency gradient switching associated with the diffusion-weighting. The artifact manifests as localized signal-loss in images acquired with partial Fourier coverage when there is a strong component of the diffusion-gradient vector in the left-right direction. This signal loss is caused by local phase ramps in the image domain which shift the apparent k-space center for a particular voxel outside the covered region. The local signal loss masquerades as signal attenuation due to diffusion, severely disrupting the quantitative measures associated with diffusion-tensor imaging (DTI). We suggest a way to improve the interpretation of affected DTI data by including a co-regressor which accounts for the empirical response of regions affected by the artifact. We also demonstrate that the artifact may be avoided by acquiring full k-space data, and that subsequent increases in TE can be avoided by employing parallel acceleration. *Hum Brain Mapp* 00:000–000, 2009. © 2009 Wiley-Liss, Inc.

Key words: diffusion imaging; DTI; vibration; artifact



INTRODUCTION

Diffusion-weighted MR imaging generates contrast that is dependent on the extent of water diffusion in the direction of the diffusion sensitization [Le Bihan et al., 1986]. The large gradient lobes employed to achieve the diffusion-weighting are known to cause vibrations of the

patient table which are noticeable to the subject. Hiltunen et al. [2006] used a laser interferometer to measure the vibrations resulting from the pulse-sequences typically used for diffusion tensor imaging (DTI), but did not quantify how the vibrations might affect the images acquired. Vibrations could be expected to have a considerable effect, however, as previous work has demonstrated the strong sensitivity of diffusion-weighted imaging to bulk motion [Anderson and Gore, 1994; Ordidge et al., 1994; Wedeen et al., 1994]. It has been demonstrated in a gel phantom that mechanical separation of the sample from the patient table can lead to substantial changes in the measured apparent diffusion coefficient [Ogura et al., 2006], but the authors appear not to have considered a mechanism for this discrepancy or whether human brain studies are likely to be affected in the same way. In this article, we identify in vivo a pronounced artifact, which we attribute to result directly from the vibrations of the patient table which

Contract grant sponsors: Vera and Volker Doppelfeld Foundation.

*Correspondence to: Daniel Gallichan, Department of Diagnostic Radiology, University Hospital Freiburg, Hugstetter Str. 55, 79106 Freiburg, Germany. E-mail: daniel.gallichan@uniklinik-freiburg.de
Received for publication 7 January 2009; Revised 7 June 2009; Accepted 11 June 2009

DOI: 10.1002/hbm.20856

Published online in Wiley InterScience (www.interscience.wiley.com).

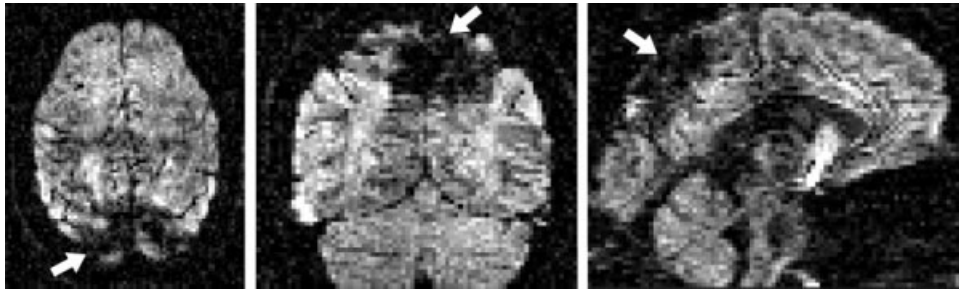


Figure 1.

Axial, coronal, and sagittal cross-sections of a diffusion-weighted volume demonstrating a severe example of the vibration artifact located mainly in the mesial parietal lobe. Diffusion-gradient direction was $[x, y, z] = [0.98, 0.02, -0.20]$.

have been induced by the low-frequency switching of the gradient coils to achieve the diffusion contrast. This artifact can lead to ambiguous interpretation of affected diffusion-weighted images as well as severe disruption of the quantitative measures derived in DTI. We propose a method to improve the analysis of the affected data by accounting for the artifact, as well as suggesting alternative pulse-sequence parameters that might be used to avoid the acquisition of data corrupted in this manner.

CHARACTERIZING THE ARTIFACT

We acquired diffusion-weighted data on a Siemens 3T TIM Trio scanner (Siemens Medical Solutions, Erlangen, Germany) fitted with a gradient coil with maximum amplitude 38 mT/m. A 12-channel head receive coil was used for all acquisitions except for those where the magnitude and phase were required, in which case a single-channel T/R head coil was used to avoid the added complexity of combining the complex data between the channels. The acquisition parameters were 2 mm isotropic resolution EPI, 192×192 mm FOV, 65 axial slices, TE/TR = 94 ms/9,300 ms, $b = 1,000$ s/mm² (using the twice-refocused spin-echo (TRSE) to reduce eddy-current related distortions [Reese et al., 2003]) and (3/4) partial Fourier imaging with phase encoding in the anterior–posterior (AP) direction. The use of partial Fourier acquisition is common in diffusion imaging to decrease the TE, which increases the signal-to-noise ratio (SNR) despite acquiring less data in k-space. The partial Fourier data was reconstructed by the default method provided by the scanner: application of an apodization filter followed by zero-padding. Two averages of 60 diffusion-gradient directions were acquired, evenly spaced on the surface of a unit sphere, along with an additional six non-diffusion-weighted volumes. All data processing was performed in Matlab (The MathWorks, Natick, MA). Figure 1 shows an example of a volume which is severely affected by the artifact, with anomalous signal loss in a large region of the mesial parietal lobe. The appearance of the artifact

was found to be highly dependent on the direction of the diffusion weighting. Figure 2 compares the measured signal in two different regions of interest (ROIs) versus the magnitude of the x -component of the diffusion-gradient direction (where the x -direction is taken to mean the left–right direction to the subject). An ROI was selected in the splenium to demonstrate the expected signal behavior in a region where the dominant direction of the white-matter fibers is left–right. A second ROI was drawn in the region of gray matter affected by the vibration artifact. The signal in the splenium ROI decreases continuously with increasing gradient in the direction of the tract, as we would expect. The signal in the artifact-affected area, however, remains constant until the x -component of the diffusion-gradient direction reaches ~ 0.75 , whereupon the signal decreases sharply. This is a region where we would ordinarily expect to see little or no dependence of the signal on the orientation of the diffusion weighting.

The strong dependence of the measured signal on the diffusion-gradient direction in regions affected by the artifact inevitably leads to errors in the diffusion-tensor fitting process. Using a standard tensor-fitting approach, areas of artifact will be interpreted as having a high FA corresponding to a tract in the left–right direction, regardless of the true direction of the dominant diffusion taking place. Figure 3a shows a directionally encoded color FA map resulting from a standard tensor-fit (linear regression) to a dataset severely affected by the diffusion artifact, demonstrating large areas that have clearly been erroneously encoded as tracts running in the left–right direction (red). Of particular note is that the regions of artifact are not restricted to the obviously affected parietal region in Figure 1, but in this case a region anterior to the corpus callosum is also falsely colored red, suggesting that errors may occur throughout the brain.

Using MedINRIA software [Toussaint et al., 2007] (<http://www.sop.inria.fr/asclepios/software/~MedINRIA/>), we tracked fibers that connect the two hemispheres in the parietal lobe. Figure 3c shows the fiber bundles that were identified using data affected by the artifact. In

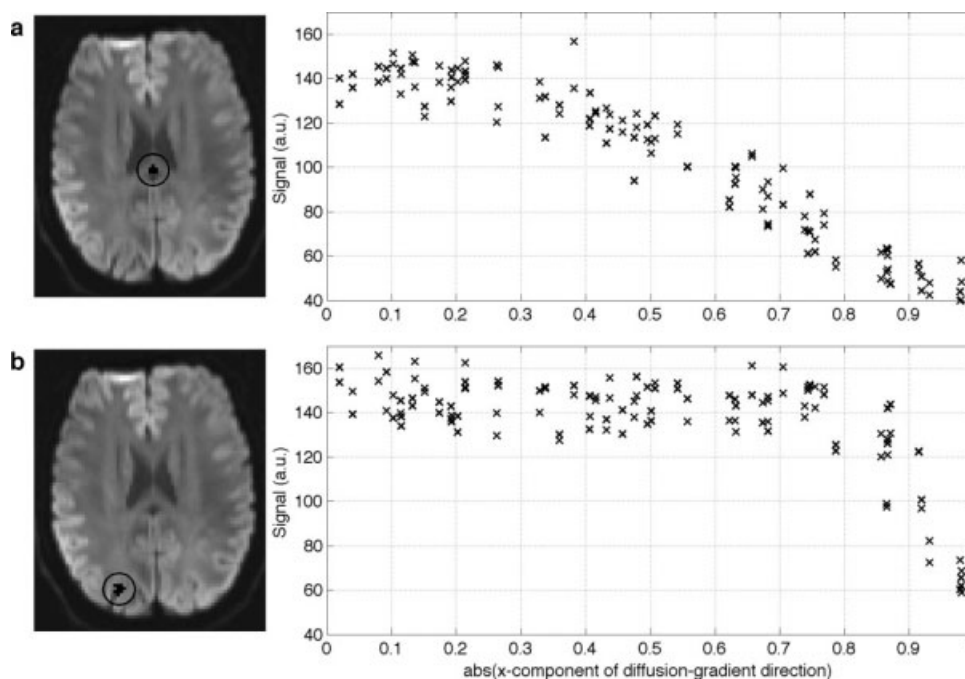


Figure 2.

Measured signal (arbitrary units) versus magnitude of x-component of diffusion-gradient direction during two repeats of a 60-direction acquisition. Plots are shown for (a) an ROI in the splenium where a white-matter tract runs in the left–right direction and (b) an ROI in gray matter affected by the vibration artifact. The images to the left show the location of the ROIs superimposed on the mean diffusion-weighted image across all directions.

addition to the appropriate connective pathway via the corpus callosum there is also a strong pathway in the left–right direction due to the artifact, which passes through gray matter and even the CSF at the mid-line of the brain. This clearly demonstrates that tractography can be strongly influenced by the presence of the vibration artifact.

Because this artifact is induced by vibrations, it is therefore dependent on the specific mechanical resonances of the scanner hardware, and will vary across different architectures. Nevertheless, occurrence of this artifact has been reported by a number of laboratories (in personal communications) and hundreds of data sets are likely to be compromised as a result.

CLINICAL SIGNIFICANCE

Diffusion-weighted EPI is used routinely to aid clinical diagnostics and decision-making, especially in stroke imaging. Typically four images are acquired, with diffusion-weighting along each of the principal axes as well as a nondiffusion-weighted image. To illustrate how diagnostic confidence might be impaired we show the example of a patient suffering from an acute ischemic stroke. The associated cytotoxic edema manifests itself as a hyperintensity on the diffusion-weighted images in all diffusion-

directions—with identification of this in all three images commonly required to confirm the diagnosis. If the region affected by the artifact overlaps with the pathology, diagnostic uncertainty can arise, which is exemplified in Figure 4. In this particular case, the cytotoxic edema coincides with the artifact region and the corresponding hyperintensity is thereby attenuated in the left/right sensitized image. Here, the interpretation remains relatively clear because it is still identifiable. However, small strokes within the mesial parietal or frontal lobe, which is also affected by the artifact in Figure 4b, are likely to cause few clinical symptoms or even to remain clinically silent. In such cases, the results of the MR examination are crucial to firmly establish the diagnosis. When overlapping with the pathological signal alterations of interest, the artifact will significantly reduce the diagnostic information available. Other clinically relevant examples would be epidermoids, abscess formations, malignancies of high cellular density such as lymphoma and inflammatory or infectious CNS diseases such as toxoplasmosis.

CAUSE OF THE ARTIFACT

Figure 5a shows a single slice acquired using the same parameters as described earlier but where both the

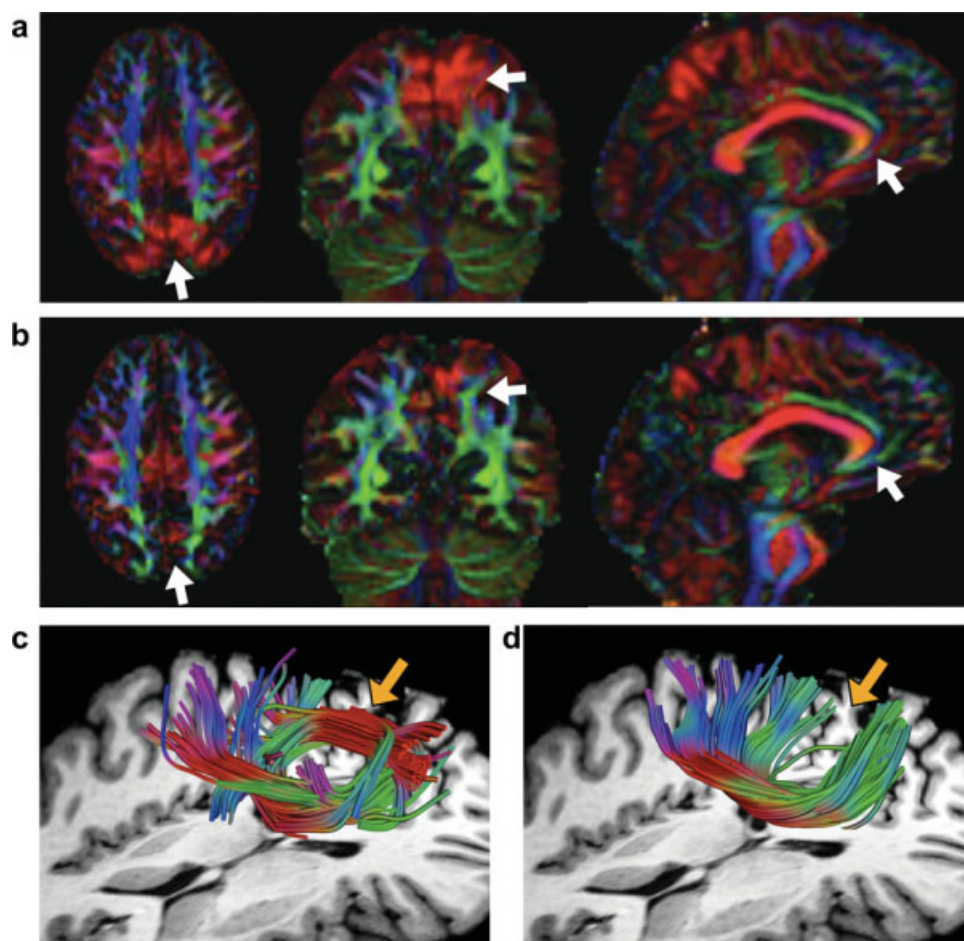


Figure 3.

(a) Axial, coronal, and sagittal cross-sections of directionally encoded color FA maps, color-coded for the direction of the first eigenvector of the fitted diffusion tensor (red—left–right, green—anterior–posterior, blue—superior–inferior) for a dataset affected by the vibration artifact. (b) The same dataset using

a tensor fit with a co-regressor to account for the artifact. (c,d) Parietal fiber bundles connecting the two hemispheres using (c) a standard diffusion-tensor fit and (d) using a co-regressor to account for the artifact.

magnitude and phase of the data were retained. The diffusion weighting was applied only in the left–right direction to focus specifically on data affected by the artifact. The phase image is shown in Figure 5b, where strong phase ramps are visible. If the brain tissue is moving in the direction of the diffusion weighting during the application of the diffusion-encoding gradients then a phase offset will occur. If neighboring voxels are moving different amounts, then this becomes a phase ramp. The strong phase ramps in Figure 5b are therefore explained by the presence of left–right mechanical shear-waves that are propagating through the brain. It has recently been demonstrated that similar vibrational waves resulting from low-frequency switching of the imaging gradients can be tracked with MRI, and used for MR elastography [Gallichan et al., 2007].

Phase ramps in image space in turn correspond to shifts in k-space, explaining the defocused spin-echo in the k-space in Figure 5c. If the apparent k-space center for a particular voxel is shifted beyond the edge of the acquired k-space, then the signal for that voxel will suddenly drop dramatically, in a similar manner to that previously observed due to bulk motion [Storey et al., 2008; Wedeen et al., 1994] or due to extra phase accrual due to concomitant field terms [Meier et al., 2008]. In our case the use of a (3/4) partial-Fourier acquisition means that the phase ramp need only reach $\pi/2$ per voxel in the anterior-to-posterior direction to experience this signal loss.

The default method to reconstruct partial-Fourier images on our scanner is to apply an apodization filter to reduce Gibbs ringing and then to zero-pad to the full matrix size before finding the inverse Fourier-transform. This

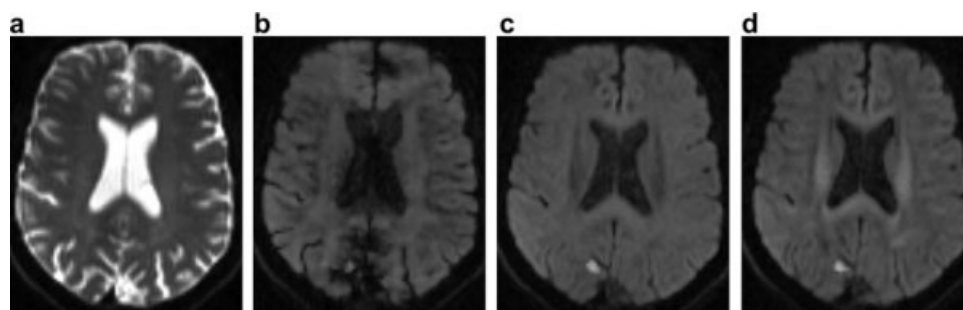


Figure 4.

Example of a clinical scan (cytotoxic edema due to acute ischemic stroke from cardiac embolism) where an isotropic decrease in the apparent diffusion is made ambiguous by the vibration artifact which affects image (b). Images are shown with (a) no diffusion-weighting as well as $b = 1,000 \text{ s/mm}^2$ in the (b) left/right,

(c) superior/inferior, and (d) anterior/posterior directions. In Routine, uniform diffusion hyperintensities in three orthogonal axes are required to confirm isotropic decreases in the apparent diffusion resulting from cytotoxic edema of an acute ischemic stroke.

apodization step slightly alters the “all-or-nothing” nature of the artifact: as the shift of the k-space center increases, the signal is attenuated before it is removed entirely. This

attenuation can make the artifact somewhat subtle, since attenuation that is not conspicuous on the raw diffusion-weighted images as a profound dropout can nevertheless

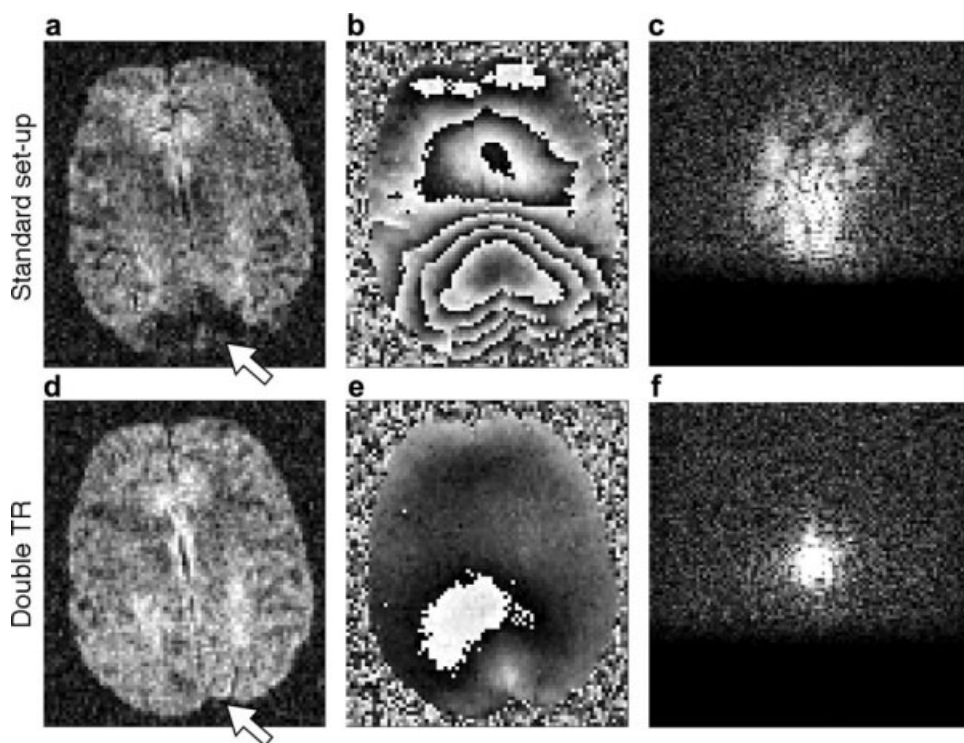


Figure 5.

Top row: (a) single axial slice of a diffusion-weighted image affected by the vibration artifact ($b = 1,000 \text{ s/mm}^2$ diffusion-weighting applied in left–right direction), along with (b) the phase image (generated without k-space apodization filter to improve phase information in low signal areas), and (c) the corresponding k-space. Bottom row: A repeat of the same acquisition as above, but with $\text{TR} = 18.6 \text{ s}$ (instead of the standard 9.3 s).

bias quantitative measures such as FA. Alternative strategies for partial-Fourier reconstruction are also likely to be affected, as it has been shown previously that strong phase variations can cause errors in partial k-space reconstruction [Robson and Porter, 1994]. Errors occur because the low-resolution phase image used in the reconstruction is a poor approximation to the rapidly altering phase. It is possible that algorithms used to combine data from multiple coils may also be affected in a similar manner.

It is interesting to note that the physical sensation of the subject is only of mildly stronger vibrations when the diffusion-weighting is applied along the left-right direction compared with the AP or superior-inferior directions. The phase of images collected with diffusion-weighting in the other two directions, however, only demonstrate mild phase variation across the brain (data not shown), with the exception of some slices collected with diffusion-weighting in the superior-inferior direction, which can occasionally show characteristic phase ramps due to motion associated with the cardiac cycle. We hypothesize that this discrepancy between the perceived vibration and the effect on the images is due to the physically resonant hardware of the scanner having a significantly longer decay time of the vibrations when excited by switching of the left-right gradient coil.

CORRECTING FOR THE ARTIFACT

Although it is understandably preferable to acquire data that are unaffected by the artifact, there are inevitably many datasets that were acquired before the recognition and characterization of the artifact. We have found that the reliability of measures such as FA can be vastly improved by including an empirically-derived approximation to the influence of the artifact as a co-regressor in the diffusion-tensor fit. Here, we briefly cover the appropriate theory to demonstrate where this co-regressor is included.

For a single voxel, the signal measured in the i th acquisition, S_i , can be written as [Basser et al., 1994]:

$$S_i = S_0 \exp(-b_i \hat{\mathbf{r}}_i^T \mathbf{D} \hat{\mathbf{r}}_i), \quad (1)$$

where S_0 is the signal that would be measured in the absence of any diffusion weighting, b is the “ b -value” which describes the magnitude of the diffusion weighting, $\hat{\mathbf{r}}_i$ is the unit vector in the direction that the diffusion-weighting was applied, and \mathbf{D} is the 3×3 diffusion tensor (which is symmetric, and therefore has six independent components). When fitting for \mathbf{D} from the measured data it is convenient to rewrite Eq. (1) in a linear matrix form:

$$\begin{pmatrix} \ln(S_1) \\ \vdots \\ \ln(S_N) \end{pmatrix} = \begin{pmatrix} -b_{xx,1} & -b_{yy,1} & -b_{zz,1} & -2b_{xy,1} & -2b_{xz,1} & -2b_{yz,1} & 1 & \ln(A(r_{x,1})) \\ \vdots & \vdots \\ -b_{xx,N} & -b_{yy,N} & -b_{zz,N} & -2b_{xy,N} & -2b_{xz,N} & -2b_{yz,N} & 1 & \ln(A(r_{x,N})) \end{pmatrix} \begin{pmatrix} D_{xx} \\ D_{yy} \\ D_{zz} \\ D_{xy} \\ D_{xz} \\ D_{yz} \\ \ln(S_0) \\ k \end{pmatrix}, \quad (2)$$

where we have also added an additional column to the multiplier matrix to include the co-regressor, $A(r_{x,i})$, which we define as a function of the x -component of $\hat{\mathbf{r}}_i$. The parameter k represents the extent to which the artifact is present in the voxel under examination. We have used the notation $b_{xy,i}$ to represent $b_i \hat{r}_{x,i} \hat{r}_{y,i}$.

It is not clear how an analytical form for $A(r_{x,i})$ could be derived from the theory which explains the nature of the artifact. We therefore chose instead to use an empirically-derived function based on the data in the regions strongly affected by the artifact. An approximate mask of the affected region was obtained by thresholding the norm of the residuals from the tensor fit. We then fit a tensor to the data from directions with $\text{abs}(r_x) < 0.6$ to obtain an estimate of the tensor unaffected by artifact. Within the mask of the affected region, the data from all directions were then divided by model data predicted from using the tensor which had been fit to a subset of directions. The result is a representation of the average artifact dependence on r_x , which is shown in Figure 6a. A smooth approx-

imation to this empirical dependence was used for $A(r_{x,i})$ in Eq. (2). It should be noted that the exact form of this function will depend in part on the reconstruction (e.g., in our case the form is dominated by the apodization function which is applied to partial k-space data). We used a Tukey windowing filter as a function which has the desired shape—constant and equal to one for low r_x magnitude and smoothly decaying for high r_x magnitudes:

$$\begin{aligned} A(r_{x,i}) &= 1 & r_{x,i} < a \\ A(r_{x,i}) &= \cos^2\left(\frac{\pi(\text{abs}(r_{x,i}) - a)}{2b}\right) & a \leq r_{x,i} \leq a + b \\ A(r_{x,i}) &= 0 & r_{x,i} > a + b \end{aligned} \quad (3)$$

where we found using least-squares fitting that $a = 0.61$ and $b = 0.54$ resulted in a good approximation to the observed artifact dependence (solid line in Fig. 6a). The same $A(r_{x,i})$ was used for all subjects.

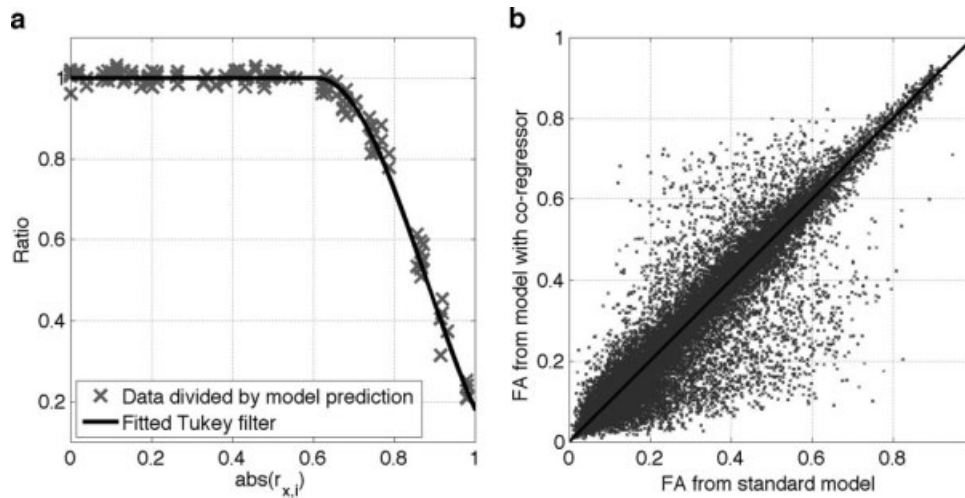


Figure 6.

(a) Ratio of measured data to predicted data [based on tensors fit to data for $\text{abs}(r_{x,i}) < 0.6$] within the artifact-affected region from a single subject. Also shown is the Tukey filter with parameters determined by a least-squares fit. (b) FA calculated by standard model versus FA calculated by model including artifact co-regressor. Data shown for $\sim 200,000$ voxels within entire brain. Solid black line indicates line of equality.

Figure 6b compares the FA values resulting from the tensor fit with and without inclusion of the artifact-related co-regressor. The data follow the line of equality closely, confirming that the co-regressor method does not introduce any other form of systematic bias in the estimation of FA.

Figure 3b shows the color-coded FA map resulting from the tensor fit which includes the artifact co-regressor for the same data as shown in Figure 3a. The volume of erroneously high FA is massively reduced, and the direction of the vectors is also largely corrected. However, a residual reddish hue is noticeable along the midline, so the correction can not be considered complete. The usefulness of the correction is further demonstrated by Figure 3d, which shows the fiber pathways identified using the same ROIs as were used to generate Figure 3c. The artifactual pathway running directly in the left–right direction between the hemispheres is completely removed by using the co-regressor to account for the vibration artifact.

Fitting with the co-regressor also allows the regions affected by the artifact to be identified more clearly, as this will be indicated by the magnitude of k . Figure 7a–c shows maximum-intensity projections of the mean value for k across 22 normal healthy subjects. The exact location of the artifact varied slightly between subjects, but was consistently strongest close to the midline of the parietal lobe. By inspecting the histogram of k values across the brain, we chose a threshold of $k > 0.5$ to indicate that the voxel is affected by the artifact. This allowed an estimation of the brain volume affected by the artifact in each subject, which is plotted in Figure 7d. There is a wide range in the

affected volume, but there was distinctly identifiable artifact in 18 out of the 22 subjects. Part of this variation might be explained by differences in the compactness of the padding used to restrain the subject, and thereby the transmission of the vibrations into the brain, as well as differences in anatomy leading to different wave magnitudes.

The co-regressor approach to correcting for the artifact is an approximation as it assumes that each voxel affected by the artifact will begin to lose signal due to the vibrations at the same threshold of r_x . We expect it may be feasible to develop an analysis approach which considers the artifact more accurately to perform a more complete correction, perhaps adapting existing outlier rejection methods such as Robust Estimation of Tensors by Outlier Rejection (RESTORE) [Chang et al., 2005]. Our aim here, however, was to develop a simple, fast and unbiased method of improving the accuracy of the tensor fit. We do not consider the correction “complete.”

The introduction of a further parameter in the tensor fitting can increase uncertainty in the tensor estimates—an effect amplified by the fact that the artifact co-regressor, $\ln(A(r_{x,i}))$, is inherently nonorthogonal to b_{xx} . It is also only possible to apply this co-regressor method to data acquired with many diffusion-gradient directions as there need to be sufficient directions in the “ramp-down” portion of the curve shown in Figure 2b to drive the parameter fit. The co-regressor method can not be applied to clinical three-direction data as there is no tensor fitting involved. For these reasons it is clearly preferable to prevent the occurrence of the artifact in data at the time of acquisition.

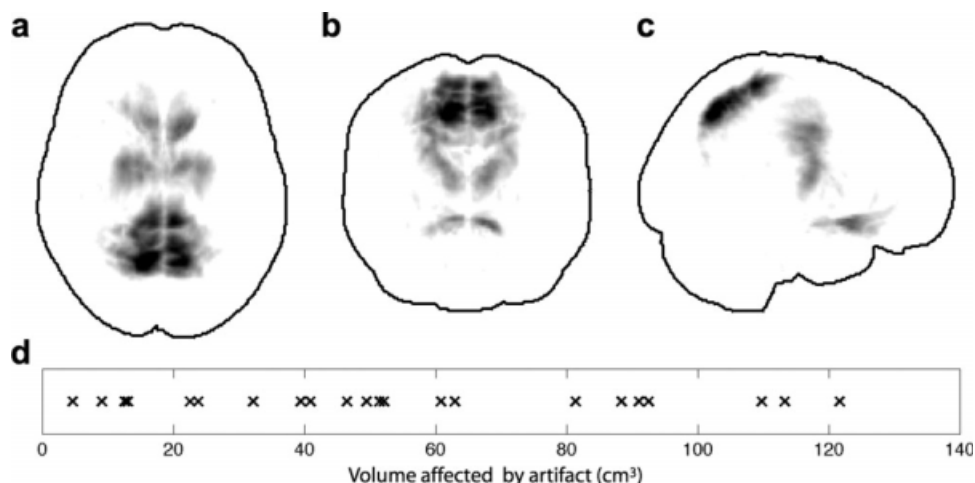


Figure 7.

Maximum-intensity projections of the mean distribution of the artifact co-regressor across 22 subjects in (a) axial, (b) coronal, and (c) sagittal views. (d) The volume of brain affected by the artifact ($k > 0.5$) in each of the 22 subjects.

AVOIDING THE ARTIFACT

As demonstrated in Figure 5, the artifact can be avoided by doubling the TR, allowing the vibrations to decay between the acquisition of each slice. This is rather an impractical solution, however, as the SNR efficiency is immediately reduced by as much as a factor of $1/\sqrt{2}$. Based on our understanding of the artifact described earlier, the simplest method to avoid acquiring affected data in a shorter acquisition time is to acquire full k-space data [instead of the (3/4) partial Fourier imaging used earlier]. If the other EPI parameters are kept constant on our system, however, this leads to a 17 ms increase in the TE from 94 to 111 ms and a corresponding increase in TR from 9.3 to 10.4 s. To avoid the SNR efficiency losses associated with these changes, parallel imaging can be used to reduce the readout duration and TE. Using GRAPPA [Griswold et al., 2002] with an acceleration factor of 2 brings the TE back down to 93 ms, whilst reducing the overall TR to 8.2 s. To demonstrate that full k-space parallel accelerated data are indeed unaffected by the vibration artifact, we performed two consecutive 30-direction acquisitions on a test subject, the first with a standard (3/4) k-space and no parallel acceleration, the second with full k-space and GRAPPA acceleration factor 2. Figure 8a compares the signal dependence on the x -component of the diffusion-gradient direction between the two acquisitions within an ROI which is affected by the artifact. As expected, the full k-space acquisition does not demonstrate the signal drop-off with strong x -gradients characteristic of the vibration artifact. To exclude the possibility that the artifact was simply displaced to a different location in the brain rather than removed entirely, Figure 8b,c show maps of the fitted co-regressor parameter k , which indicates the

presence of artifact, for the two acquisitions. The artifact-affected region is clearly visible in the (3/4) k-space acquisition, whereas the full k-space acquisition shows no regions which distinguish themselves from background noise.

Parallel imaging is typically associated with an SNR penalty as less data are acquired. However, we found that when the reduced blurring due to the full k-space coverage is accounted for (by blurring the accelerated data to match the resolutions), the SNR of the resulting images was actually slightly increased for the accelerated data (22.7 vs. 18.3 in the nondiffusion-weighted image, measured as average white matter signal divided by standard deviation of background noise).

Besides increasing the k-space coverage, another approach to avoid the artifact would be to reduce the amplitude of the mechanical vibrations within the brain. We have found that the padding used to restrain the subject's head during the scan has a large influence on the artifact—the amplitude of the brain vibrations is much reduced when no pads are placed on the sides of the head between the headphones and the coil. This can be explained by the strong mechanical coupling which tight side padding can produce in the left-right direction—the same orientation as the vibrations which lead to the artifact. However, removal of the side padding entirely is not sufficient to avoid the artifact completely. It is possible that careful design of the under-head cushion and head restraint would allow sufficient damping of the vibrations to perform artifact free imaging, but none of the padding we had available was able to achieve this.

A further solution would be to alter the mechanical resonances of the system, or how the patient table is mechanically coupled to the gradient coils. This was

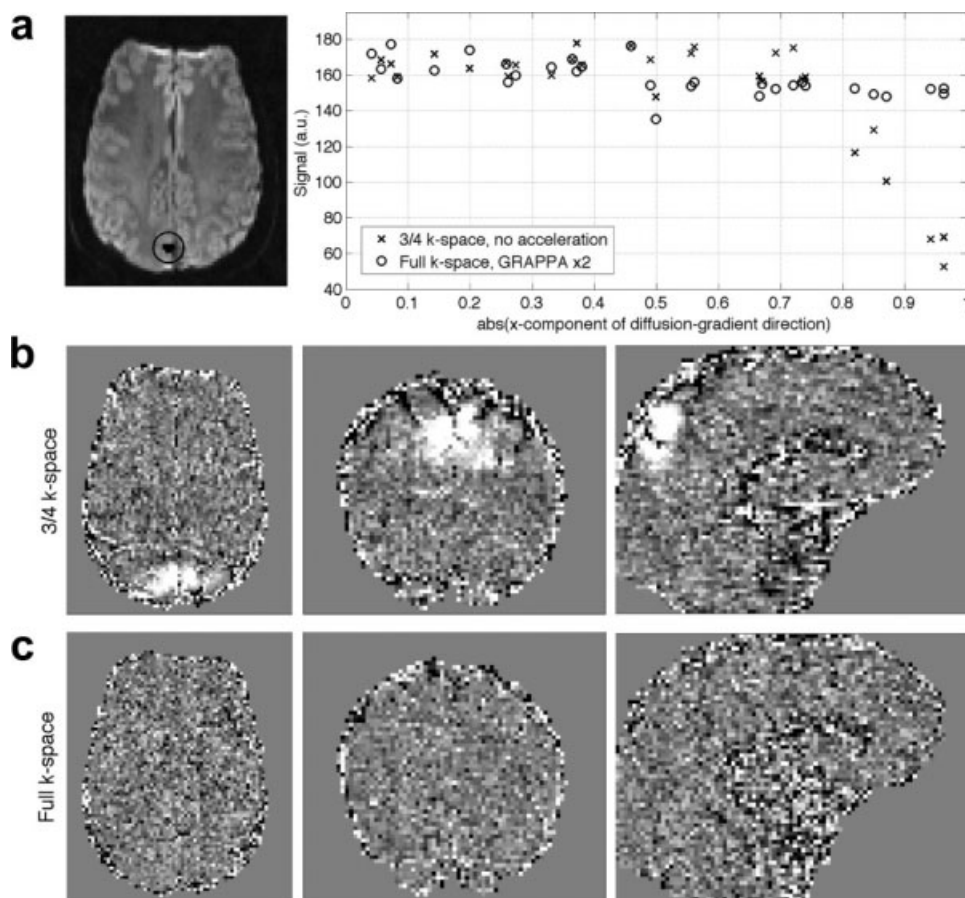


Figure 8.

(a) Measured signal (arbitrary units) versus magnitude of x -component of diffusion-gradient direction using a 30-direction acquisition within a gray-matter ROI. Crosses show data using standard imaging parameters (3/4 k-space, no acceleration) and circles show data using full k-space and a GRAPPA acceleration

factor of 2. Calculated FA: 0.45 versus 0.14, calculated ADC: 1.17 versus 1.34 mm^2/s . (b,c) Axial, coronal, and sagittal views of the fitted artifact-related parameter k for (b) the 3/4 k-space data and (c) the full k-space data.

demonstrated by Ogura et al. [2006] on a phantom by suspending the phantom within the coil attached to an apparatus not in direct contact with the MR system. Such an extreme approach is likely to be impractical for in vivo scanning, but manufacturers may wish to consider these low-frequency resonances when designing new hardware and new systems.

CONCLUSION

We have identified a pronounced artifact affecting diffusion-weighted imaging which arises due to the vibrations in the patient table resulting from the low-frequency gradient switching necessary to apply the diffusion-weighting. We have suggested a method that can be used to improve the analysis of DTI data affected by the artifact which uses a co-regressor based on the empirical dependence of the signal on the magnitude of the component of the diffu-

sion-gradient vector in the left–right direction. We have also demonstrated that acquiring full k-space data is sufficient to avoid the artifact, and that the associated TE increase can be avoided by employing parallel acceleration without an SNR penalty in the resolution-matched images.

REFERENCES

- Anderson AW, Gore JC (1994): Analysis and correction of motion artifacts in diffusion weighted imaging. *Magn Reson Med* 32:379–387.
- Basser PJ, Mattiello J, Le Bihan D (2005): MR diffusion tensor spectroscopy and imaging. *Biophys J* 66:259–267.
- Chang L, Jones D, Pierpaoli C (2005): RESTORE: Robust estimation of tensors by outlier rejection. *Magn Reson Med* 53:1088–1095.

- Gallichan D, Robson M, Bartsch A, Miller K (2009): TREMR: Table-resonance elastography with MR. *Magn Reson Med* (in press).
- Griswold MA, Jakob PM, Heidemann RM, Nittka M, Jellus V, Wang J, Kiefer B, Haase A (2002): Generalized autocalibrating partially parallel acquisitions (GRAPPA). *Magn Reson Med* 47:1202–1210.
- Hiltunen J, Hari R, Jousmäki V, Müller K, Sepponen R, Joensuu R (2006): Quantification of mechanical vibration during diffusion tensor imaging at 3 T. *Neuroimage* 32:93–103.
- Le Bihan D, Breton E, Lallemand D, Grenier P, Cabanis E, Laval-Jeantet M (1986): MR imaging of intravoxel incoherent motions: Application to diffusion and perfusion in neurologic disorders. *Radiology* 161:401–407.
- Meier C, Zwanger M, Feiweier T, Porter D (2005): Concomitant field terms for asymmetric gradient coils: Consequences for diffusion, flow, and echo-planar imaging. *Magn Reson Med* 60:128–134.
- Ogura A, Maeda F, Miyai A, Hayashi K, Hongoh T (2006): Effect of vibration caused by time-varying magnetic fields on diffusion-weighted MRI. *Nippon Hoshasen Gijutsu Gakkai zasshi* 62:565–569.
- Ordidge R, Helpert J, Qing Z, Knight R, Nagesh V (1994): Correction of motional artifacts in diffusion-weighted MR images using navigator echoes. *Magn Reson Imaging* 12:455–460.
- Reese TG, Heid O, Weisskoff RM, Wedeen VJ (2003): Reduction of eddy-current-induced distortion in diffusion MRI using a twice-refocused spin echo. *Magn Reson Med* 49:177–182.
- Robson MD, Porter DA (1994): Reconstruction as a source of artifact in non-gated single-shot diffusion-weighted EPI. *Magn Reson Imaging* 23:899–905.
- Storey P, Frigo F, Hinks RS, Mock B, Collick B, Baker N, Marmurek J, Graham SJ (2008): Partial k-space reconstruction in single-shot diffusion-weighted echo-planar imaging. *Magn Reson Med* 57:614–619.
- Toussaint N, Souplet J, Fillard P (2007): MedINRIA: DT-MRI Processing and Visualization Software. Brisbane, Australia: Proceedings of MICCAI'07 Workshop on interaction in medical image analysis and visualization.
- Wedeen VJ, Weisskoff RM, Poncelet BP (1994): MRI signal void due to in-plane motion is all-or-none. *Magn Reson Med* 32:116–120.